Journal of Theoretical Biology 462 (2019) 432–445

Contents lists available at ScienceDirect

Journal of Theoretical Biology

journal homepage: www.elsevier.com/locate/jtb

Origins of oscillation patterns in cyclical thrombocytopenia

Changjing Zhuge[b], Michael C. Mackey[a], Jinzhi Lei[c,*]

[a] Departments of Physiology, Physics & Mathematics, McGill University, 3655 Promenade Sir William Osler, Montreal, Quebec H3G 1Y6, Canada
[b] Beijing Institute for Scientific and Engineering Computing, Beijing University of Technology, Beijing 100124, China
[c] Zhou Pei-Yuan Center for Applied Mathematics, MOE Key Laboratory of Bioinformatics, Tsinghua University, Beijing 100084, China

ARTICLE INFO

Article history:
Received 15 June 2018
Revised 22 November 2018
Accepted 26 November 2018
Available online 27 November 2018

2010 MSC:
92C50
34K60
34K18

Keywords:
Hematopoiesis
Cyclical thrombocytopenia
Cyclical neutropenia
Bifurcation analysis
Delay differential equation

ABSTRACT

Cyclical thrombocytopenia (CT) is a rare hematological disease characterized by periodic oscillations in circulating platelet counts. In almost all CT patients, other cell lines show no sign of oscillation, but recently a CT patient was reported with significant oscillations in circulating neutrophils (in the same period as the platelets). In this paper, we attempt to understand this phenomenon through a previously published model of human hematopoiesis. We have investigated a variety of possible oscillation patterns that may appear when alterations occur in the control parameters in the platelet regulatory dynamics. Our results indicate that the platelet maturation time and the differentiation rate from hematopoietic stem cells (HSCs) into the platelet cell line play important roles in the emergence of various types of CT like oscillations. Moreover, we find different oscillation patterns, including CT and cyclical neutropenia like oscillations, with certain parameter values in the platelet compartment. A bifurcation analysis revealed the different origins of these oscillation patterns. We also identified bistable dynamics which indicate the potential importance of system history in the treatment of these diseases. Together, these results demonstrate the possible origins for various oscillation patterns dependent on alterations in the platelet cell line control mechanisms. One of the important origins may be related to the regulation of apoptosis in platelet precursors.

© 2018 Published by Elsevier Ltd.

1. Introduction

All mature circuiting blood cells arise from morphologically undifferentiated cells in the bone marrow, that is, from the hematopoietic stem cells (HSCs). HSC can either self-renew or differentiate to produce all types of blood cells (erythrocytes, neutrophils, platelets, *etc.*). Hematopoiesis is a homeostatic system controlled by feedbacks mediated by various hematopoietic cytokines, such as erythropoietin (EPO) which mediates erythrocyte (or red blood cell, RBC) production, granulocyte colony stimulation factor (G-CSF), which controls the regulation of neutrophil production, and thrombopoietin (TPO), which is the primary regulator of thrombopoiesis and platelet production. Dysregulation in this control system can lead to failures in the homeostatic maintenance in one or more blood cell lines (Foley and Mackey, 2009; Hoggatt et al., 2016; Lei and Mackey, 2014; MacLean et al., 2014; Morales-Mantilla and King, 2018).

Periodic hematological disorders are classic examples of dynamical diseases (Glass and Mackey, 1988) characterized by oscillations in cell counts of one or more circulating blood cells with periods ranging from days to months (Dale and Mackey, 2015; Haurie et al., 1998). Some diseases show oscillations in all major blood cell lines, such as cyclical neutropenia (CN), with its characteristic ELANE mutation in the gene for neutrophil elastase (Haurie et al., 1998; 1999; Horwitz et al., 1999), and periodic chronic myeloid leukemia (PCML) (Fortin and Mackey, 1999; Safarishahrbijari and Gaffari, 2013), believed to arise in the stem cell compartment because of the presence of the Philadelphia chromosome mutation (Seong et al., 1998). In other diseases, such as periodic auto-immune hemolytic anemia (AIHA, Mackey (1979)) and cyclical thrombocytopenia (CT, Swinburne and Mackey, 2000), most patients show oscillations in only one cell type, and cell counts in other cell lines are normal, suggesting potentially alternative mechanisms for the disease origin.

CT is a rare hematological disorder characterized by periodic cycling in platelet counts (Kosugi et al., 1994; Pavord et al., 1996; Sekine et al., 1989; Swinburne and Mackey, 2000; Wahlberg et al., 1977). This disorder is characterized by a variety of symptoms including purpura, petechiae, epistaxis, gingival bleeding, menorrhagia, and easy bruising. In normal subjects, circulating platelet levels remain relatively stable for years ($150 - 450 \times 10^9$ platelets/L, with an average of 290×10^9 platelets/L). However, in CT patients

* Corresponding author.
E-mail addresses: zhuge@bjut.edu.cn (C. Zhuge), michael.mackey@mcgill.ca (M.C. Mackey), jzlei@tsinghua.edu.cn (J. Lei).

https://doi.org/10.1016/j.jtbi.2018.11.024
0022-5193/© 2018 Published by Elsevier Ltd.

the platelet counts oscillate from very low (1×10^9 platelets/L) to normal or very high levels (2000×10^9 platelets/L), with periods varying from 13 days to 65 days among different patients (Swinburne and Mackey, 2000).

In *all previously known* CT cases the oscillations appear only in the platelets and not in the white or red blood cells (Apostu and Mackey, 2008; Swinburne and Mackey, 2000). However, a recent case report of CT documents statistically significant oscillations in neutrophil counts with the same period (39 days) as the platelet oscillation (Langlois et al., 2018). The patient studied by Langlois et al. (2018) tested negative for the presence of the ELANE mutation that is characteristic of cyclical neutropenia (Horwitz et al., 1999) hence, it was not a case of misdiagnosis. *This observation intrigued us and led to the present paper.*

Despite a long history of modeling of hematopoietic dynamics (Adimy et al., 2014; Dale and Mackey, 2015; Foley and Mackey, 2009; Lei and Mackey, 2014; MacLean et al., 2014; Mouser et al., 2014; Pujo-Menjouet, 2016; Roeder et al., 2009; Traulsen et al., 2013; Whichard et al., 2010), the pathogenesis of CT is poorly understood. Previous modeling efforts have indicated that alterations in control parameters can lead to bifurcations in system dynamics in the genesis of periodic hematological diseases. However, the precise nature of the underlying alteration varies depending on the model being studied.

An early mathematical approach used to try to understand CT was proposed by Santillán et al. (2000). Later, Apostu and Mackey (2008) expanded this approach incorporating an assumption of megakaryocyte deficiency and cyclical failure in platelet production (amegakaryocytic CT), but they did not suggest that oscillations in platelet levels could be accompanied by oscillations in neutrophil levels. A more recent publication (Langlois et al., 2017) considered only the regulation of platelet production and concluded that the primary change in cyclic thrombocytopenia is an interference with, or destruction of, the thrombopoietin receptor, with secondary changes in other processes, including immune-mediated destruction of platelets, megakaryocyte deficiency, and failure in platelet production.

In this study, we use an extension of previous mathematical models of hematopoiesis (Apostu and Mackey, 2008; Colijn and Mackey, 2005a; 2005b; Lei and Mackey, 2011; Zhuge et al., 2012) to examine the possible origins of CT and, in particular, the possibility of concomitant neutrophil oscillations as reported in Langlois et al. (2018). Based on the proposed model, we investigate oscillation patterns that may be associated with CT.

The outline of the paper is as follows. The mathematical model is introduced in Section 2, where we also specify the parameters from previous studies that we used along with new parameters that had to estimated. Based on model simulations, we show that a variety of oscillatory patterns are possible; we present our study of how these patterns are dependent on model parameters in Section 3.1. To verify the model, we fit simulations with Langlois et al. (2018) patient data in Section 3.2. In Section 3.3, we study the oscillation patterns by carrying out a bifurcation analysis to further examine the role of various model components in generating the behavior observed numerically. The paper concludes with a short Section 4 that summarizes our results.

2. Model development

2.1. Model description

Fig. 1shows a cartoon representation of the model in this paper. We established model equations to examine the possible origin for the concomitant occurrence of oscillations in neutrophil and platelet levels as reported in Langlois et al. (2018). The model is based on previous studies and consists of three compartments

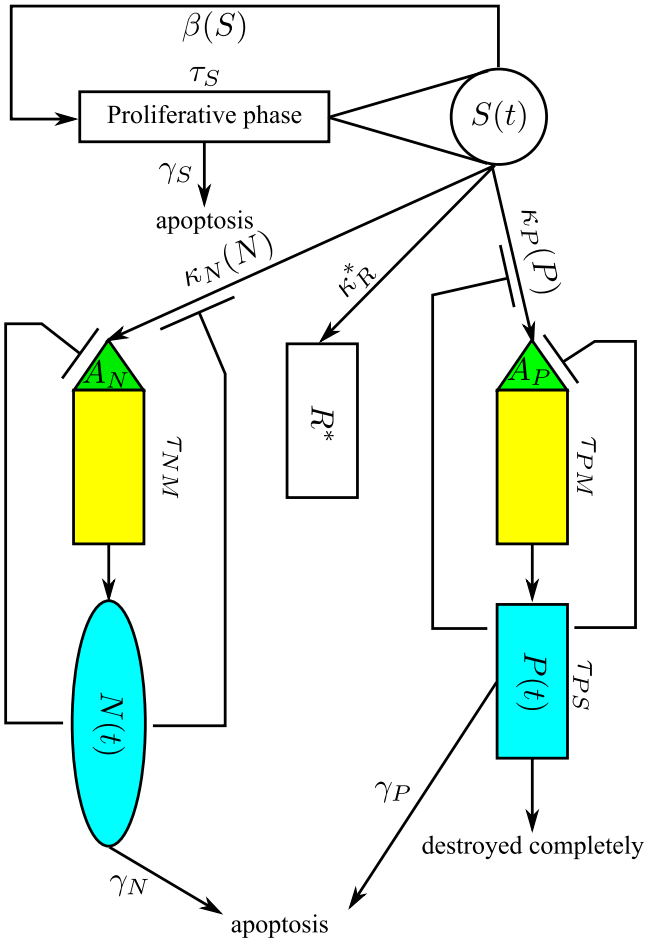

Fig. 1. Schematic representation of the mathematical model of hematopoiesis. The model includes the hematopoietic stem cells (HSC) ($S(t)$), neutrophils ($N(t)$), erythrocytes ($R(t)$) and platelets ($P(t)$). Resting phase HSCs either remain quiescent, exit into the proliferative phase at a rate β, or differentiate into one of the committed blood cell lines. Cells in the HSC proliferative phase are assumed to undergo apoptosis at a rate γ_S during a period τ_S. Each of the differentiated blood cell compartments are further divided into three subcompartments: proliferating (green), maturating (yellow), and circulating (blue) cells. The differentiation rates are κ_N, κ_P, and κ_R, respectively. Neutrophil precursors are amplified at a rate A_N, followed by maturation for a total period of time τ_{NM} before they enter the circulation. The circulating neutrophils randomly die at a rate γ_N. Platelet numbers are amplified at a rate A_P by a series of nuclear divisions and undergo maturation during a time period τ_{PM} before being released into the circulation. Circulating platelets randomly die at a rate γ_P, and are destroyed at time τ_{PS} after entering the circulation.

(Apostu and Mackey, 2008; Colijn and Mackey, 2005a; 2005b; Zhuge et al., 2012): the hematopoietic stem cells (HSC), the neutrophils (N), and the platelets (P). The current study was intended to investigate the origin of CT; hence, we did not initially include the dynamics of erythrocyte production in the model and assumed that the differentiation rate from HSCs to erythrocytes is a constant κ_R^* (days $^{-1}$). In previous models of the full hematopoiesis dynamics (Colijn and Mackey, 2005a), mature red blood cells regulated the erythrocyte differentiation through a feedback with a delay (more than 120 days) which is much longer than the period of CT oscillations, leading us to believe that the effect can be neglected in the current study. We have compared simulated dynamics based on models with and without the erythrocyte compartment, which shows this to be the case (Appendix C), and (thus our simplification of neglecting the erythrocyte compartment seems justified.

We employed a classical G_0 phase cell cycle model for the stem cells (Burns and Tannock, 1970). The HSCs are classified as either quiescent (resting G_0 phase, $S(t)$) or proliferative phase cells. Quies-

cent phase HSCs can either enter the proliferative phase at a rate β (days^{-1}) or differentiate into the precursors of any of the three cell lines: neutrophils, erythrocytes, or platelets. The rate of re-entry into the proliferative phase β depends on the number of resting phase HSCs through a negative feedback described by a Hill function (Bernard et al., 2003; Mackey, 1978)

$$\beta(S) = k_0 \frac{\theta_2^{s_2}}{\theta_2^{s_2} + S^{s_2}}, \tag{1}$$

where k_0 is the maximal re-entry rate and θ_2 is such that $\beta(\theta_2) = k_0/2$. Cells in the HSC proliferative phase are assumed to undergo apoptosis at a rate γ_S (days^{-1}), and the duration of the proliferative phase is τ_S (days). Each proliferative phase cell that survives to mitosis generates two quiescent phase cells.

The neutrophil and platelet compartments were further subdivided into three subcompartments that correspond to proliferating, maturating, and circulating cells.

After differentiation from the HSC, the neutrophil precursors are amplified by a factor A_N through successive mitotic divisions, followed with maturation before release into the circulation. The total time spent in amplification and maturation is τ_{NM} (days). Circulating neutrophils randomly die at a rate γ_N (days^{-1}).

In the platelet compartment, cells undergo a series of divisions until reaching the megakaryocyte stage where the cells no longer proliferate but undergo endoreduplication. The total amplification is given by A_P and a megakaryocyte needs τ_{PM} days to mature and release platelets into circulation. Circulating platelets randomly die at a rate γ_P (days^{-1}). In addition, circulating platelets are assumed to have a fixed lifetime τ_{PS} after entering circulation.

The model introduced by Colijn and Mackey (2005a) assumed that circulating blood cells repress the differentiation of HSC to their own precursors via cytokine interactions, and the differentiation rates κ_N and κ_P were formulated as Hill functions

$$\kappa_N(N) = f_0 \frac{\theta_1^{s_1}}{\theta_1^{s_1} + N^{s_1}}, \tag{2}$$

$$\kappa_P(P) = \frac{\bar{\kappa}_P}{1 + K_P P^{s_4}}. \tag{3}$$

Note that this assumption for the platelets was introduced by Colijn and Mackey (2005a), and was subsequently discarded by Apostu and Mackey (2008), as they considered CT with oscillations only in the platelet compartment. Here, we kept the assumptions in Colijn and Mackey (2005a) because the state-dependent differentiation rate is more realistic since the platelets regulate the differentiation of HSCs into their precursors through megakaryocytes (Chang et al., 2007; Kaushansky and Zhan, 2018; Nakamura-Ishizu et al., 2014). Moreover, the case report in Langlois et al. (2018) suggests that the platelet dynamics might interact with the other cell lines.

The dimensionless amplification factors A_N and A_P reflect the *net* proliferation following cell division and apoptosis of precursors formulated as follows.

$$A_N(N) = A_{N,\max} e^{-\eta_N \tau_{NM}}, \tag{4}$$

$$A_P(P) = A_{P,\max} e^{-\eta_P \tau_{PM}}, \tag{5}$$

where η_N and η_P are the apoptosis rates of the neutrophil and platelet precursors, respectively. Here, as in Langlois et al. (2017), we have assumed that the net precursor amplification is regulated by mature blood cell counts so that the proliferation rates are decreasing functions of the corresponding mature cell counts. This can be correspondingly interpreted that the apoptosis rates η_N and η_P are increasing functions of N and P, respectively, which are represented with Hill type functions:

$$\eta_N(N) = \bar{\eta}_N \frac{N^{\nu_1}}{\vartheta_1^{\nu_1} + N^{\nu_1}}, \tag{6}$$

$$\eta_P(P) = \bar{\eta}_P \frac{P^{\nu_4}}{\vartheta_4^{\nu_4} + P^{\nu_4}}. \tag{7}$$

These considerations lead to the following set of delay differential equations for the three model components of the HSC, the neutrophils, and the platelets (Apostu and Mackey, 2008; Colijn and Mackey, 2005a; 2005b):

$$\begin{aligned} \frac{dS}{dt} &= -(\beta(S) + \kappa_N(N) + \kappa_P(P) + \kappa_R^*)S \\ &\quad + 2e^{-\gamma_S \tau_S} \beta(S_{\tau_S}) S_{\tau_S} \end{aligned} \tag{8}$$

$$SNP\ Model: \frac{dN}{dt} = -\gamma_N N + A_N(N_{\tau_{NM}}) \kappa_N(N_{\tau_{NM}}) S_{\tau_{NM}} \tag{9}$$

$$\begin{aligned} \frac{dP}{dt} &= -\gamma_P P + A_P(P_{\tau_{PM}}) \Big(\kappa_P(P_{\tau_{PM}}) S_{\tau_{PM}} \\ &\quad - e^{-\gamma_P \tau_{PS}} \kappa_P(P_{\tau_{PSum}}) S_{\tau_{PSum}} \Big), \end{aligned} \tag{10}$$

where $\tau_{Psum} = \tau_{PM} + \tau_{PS}$. We denote this as the *SNP* (stem cell, neutrophil, platelet) model. Hereafter we always use the convention that a variable delayed by a time τ, that is, $x(t - \tau)$ is denoted by x_τ.

2.2. Reduced models

The *SNP* model that couples the three cell lines is basic to the discussions below. To better understand and analyze the core origin of CT, we omit specific feedbacks to decouple the compartments and obtain reduced models. First, by assuming a constant neutrophil count ($N(t) \equiv N_*$) in (8), we reduced the original *SNP* model to an *SP* model for the dynamics of the HSC and platelet compartments:

$$\frac{dS}{dt} = -(\beta(S) + \kappa_P(P) + \kappa_0)S + 2e^{-\gamma_S \tau_S} \beta(S_{\tau_S}) S_{\tau_S} \tag{11}$$

$$\begin{aligned} SP\ Model: \frac{dP}{dt} &= -\gamma_P P + A_P(P_{\tau_{PM}}) \Big(\kappa_P(P_{\tau_{PM}}) S_{\tau_{PM}} \\ &\quad - e^{-\gamma_P \tau_{PS}} \kappa_P(P_{\tau_{PSum}}) S_{\tau_{PSum}} \Big), \end{aligned} \tag{12}$$

where $\kappa_0 = \kappa_N(N_*) + \kappa_R^*$.

We also considered the equation for the dynamics of HSC alone by assuming constant neutrophil and platelet levels, which yields the *S* model:

$$S\ Model: \frac{dS}{dt} = -(\beta(S) + \kappa)S + 2e^{-\gamma_S \tau_S} \beta(S_{\tau_S}) S_{\tau_S}, \tag{13}$$

where $\kappa = \kappa_N(N_*) + \kappa_P(P_*) + \kappa_R^*$, and similarly, the dynamics of platelets alone by assuming constant HSC counts $S(t) \equiv S_*$, which yields the *P* model:

$$P\ Model: \frac{dP}{dt} = -\gamma_P P + A_P(P_{\tau_{PM}}) S_* \Big(\kappa_P(P_{\tau_{PM}}) - e^{-\gamma_P \tau_{PS}} \kappa_P(P_{\tau_{PSum}}) \Big). \tag{14}$$

2.3. Model parameters

In this study, most model parameters in HSC and the neutrophil compartments were taken from Colijn and Mackey (2005a) and Zhuge et al. (2012), and parameters in the platelet compartment were from Lei and Mackey (2011). Parameters related to the apoptosis rates of precursors (those in Eqs. (6) and (7)) were calculated from Langlois et al. (2017). All parameter values are listed in Table 1, and their determinations are detailed in Appendix A.

Table 1
Normal steady state parameters.

Parameter name	Value used	Unit	Sources
Stem cell compartment (S)			
S_*	1.1	$\times 10^6$cells/kg	1
γ_S	0.1	days^{-1}	1
τ_S	2.8	days	1
k_0	3.0	days^{-1}	1
θ_2	0.5	$\times 10^6$cells/kg	1
s_2	4	(none)	1
Neutrophil compartment (N)			
N_*	6.9	$\times 10^8$cells/kg	1, 2
γ_N	2.4	days^{-1}	1, 2
τ_{NM}	3.5	days	1
$A_{N,\max}$	70635	(none)	Calculated from 2
$\bar{\eta}_N$	0.27	days^{-1}	2
f_0	0.40	days^{-1}	1, 2
θ_1	0.36	$\times 10^8$cells/kg	1, 2
s_1	1	(none)	1, 2
ϑ_1	79.7	$\times 10^8$cells/kg	Assumption
ν_1	1	(none)	Assumption
Erythrocyte compartment			
κ_R^*	0.00469	days^{-1}	Calculated from 1
Platelet compartment (P)			
P_*	3.1071	$\times 10^{10}$cells/kg	3
γ_P	0.05	days^{-1}	3
τ_{PM}	7	days	1, 4
τ_{PS}	9.5	days	1, 4
$\bar{\kappa}_P$	0.372	days^{-1}	Calculated from 3
$A_{P,\max}$	2^{19}	(none)	Assumption based on 3
$\bar{\eta}_P$	0.55	days^{-1}	Calculated based on 3
K_P	11.66	$(10^{10}$ cells/kg $)^{-s_4}$	1, 4
s_4	1.29	(none)	1, 4
ϑ_4	35.9	$\times 10^{10}$cells/kg	Calculated from 3
ν_4	1	(none)	Calculated from 3

Sources: 1 = Colijn and Mackey (2005a), 2 = Zhuge et al. (2012), 3 = Langlois et al. (2017), 4 = Lei and Mackey (2011). Details are described in Appendix A.

2.4. Methods

The delay differential models were solved numerically, with given set of parameters, through WOLFRAM MATHEMATICA.

To explore the dependence of model dynamics with a set of parameters, we altered the parameters randomly within 1/30 to 30 of their default values, and sampled them uniformly in log scale (e.g., for $\bar{\kappa}_P$ and τ_{PM}, the $\log\bar{\kappa}_P$ and $\log\tau_{PM}$ were taken random bellowing the uniform distribution), but other parameters were fixed to their default values to perform model simulation (Fig. 2a).

In fitting the experimental data, we were not trying to fit each discrete data point. Instead, we applied the genetic algorithm to identify parameters to fit the characteristic measurements of oscillation dynamics in the clinical data. Details are shown in Appendix D and the parameters for fitting patient data are shown in Table 3.

The bifurcation analysis in Section 3.3 was carried out using MATLAB® package DDE-BIFTOOL (Engelborghs et al., 2002; Sieber et al., 2014).

All source codes are available in the Supplemental Material.

3. Results

3.1. Different patterns of cellular dynamics

To study the dynamic behavior of this model, we introduced perturbations to the parameters in the platelet compartment control and investigated the system dynamics. With their model, Apostu and Mackey (2008) observed that the period of the platelet oscillation was dependent on the platelet maturation time τ_{PM}. Cyclical thrombocytopenia is characterized by significant fluctuations in the platelet counts. Hence, to explore their effects on the platelet dynamics, we considered how the model dynamics depend on the parameters $\bar{\kappa}_P$ and τ_{PM} (Fig. 2a). According to model simulations, increasing the maturation time τ_{PM} results in relatively small amplitude oscillations in the platelet counts (Fig. 2c–d), while increasing the maximum differentiation rate $\bar{\kappa}_P$ yields larger amplitude oscillations in the platelet counts (Fig. 2e). Note that, in Fig. 2d–e, there are oscillations in both stem cell and neutrophil counts. In Fig. 2d, which corresponds to increases in both τ_{PM} and $\bar{\kappa}_P$, neutrophils show small amplitude oscillations with high nadirs. In Fig. 2e, neutrophil oscillations show large amplitudes with a low-level nadir, somewhat akin to the dynamics of cyclical neutropenia (Colijn and Mackey, 2005a; Lei and Mackey, 2011).

The nadirs of neutrophils are crucial for patients because low level neutrophil counts are often associated with severe neutropenia and immune-deficient symptoms that may cause death. Therefore, we further examined the dependence of neutrophil nadirs on the parameters τ_{PM} and $\bar{\kappa}_P$ (Fig. 2b). A clear separation occurs between a high neutrophil nadir ($> 2.3\times10^8$ cell/kg) and low nadirs. From Fig. 2b, low neutrophil nadirs correspond to an increase in $\bar{\kappa}_P$, and the parameter region of low neutrophil counts is in accordance with the region of large platelet amplitude (Fig. 2a and b). These results suggest a possible association between the large amplitude platelet oscillations and low level neutrophil nadirs (to be detailed below).

To further investigate the effects of perturbations in the platelet compartment on the full system, we further explored the dependence of oscillation patterns with all key regulation parameters in platelet compartment ($\bar{\kappa}_P$, $\bar{\eta}_P$, τ_{PS}, τ_{PM}, γ_P, ϑ_4 and $A_{P,\max}$). For each parameter set with oscillatory dynamics, we calculated the periods using the Lomb-Scargle periodogram technique (Lomb, 1976), neutrophil nadirs, and relative amplitudes of platelets and neutrophils (the ratio of the amplitude to the average level, Fig. 3). Despite perturbations in all 7 parameters, an obvious separation occurs in the neutrophil nadirs at a boundary of approximately 2×10^8 cells/kg (Fig. 3a), similar to previous observations with perturbations to the two parameters τ_{PM} and κ_P (Fig. 2b). Comparing Figs. 3a with b, parameters with high (blue dots) and low (red dots) level neutrophil nadirs correspond to small and large relative amplitudes of neutrophils, respectively, except for a few exceptions in the transition region. These observations suggest a classification of oscillatory dynamics based on the neutrophil nadirs: Pattern 1 when the neutrophil nadir is larger than 2.3×10^8 cell/kg (blue dots), and Pattern 2 for smaller neutrophil nadirs (red dots) (Fig. 3a). Based on the random platelet compartment parameters, we calculated the percentage of parameters with a low neutrophil nadir ($< 2.3\times10^8$ cell/kg) in accordance with various relative amplitudes of HSC and platelets, and the percentage is increased with the relative amplitude (Fig. 3c).

For Pattern 1 oscillations, most cases have large relative amplitudes in platelet oscillations and small relative amplitudes in the neutrophil oscillation (< 0.1), similar to the dynamics observed in cyclical thrombocytopenia. An example is shown in Fig. 2c. Nevertheless, cases have occurred in which there are obvious oscillations in neutrophils (relative amplitudes between 0.1 and 1.0), as shown in Fig. 2d.

Typical cyclical thrombocytopenia patients show significant oscillations in platelets and no oscillation in neutrophils (Apostu and Mackey, 2008), but a recent case report studied a patient with oscillations in both platelets and neutrophils (Langlois et al., 2018). Pattern 1 oscillations in our model simulations reproduced these two types of dynamics: most perturbations in the platelet compartment showed typical dynamics with no (or low amplitude) oscillation in the neutrophils, and in rare situations, we saw oscillations in both platelets and neutrophils. Hence, we further divided the Pattern 1 oscillations into two subclasses, Pattern 1a (typical

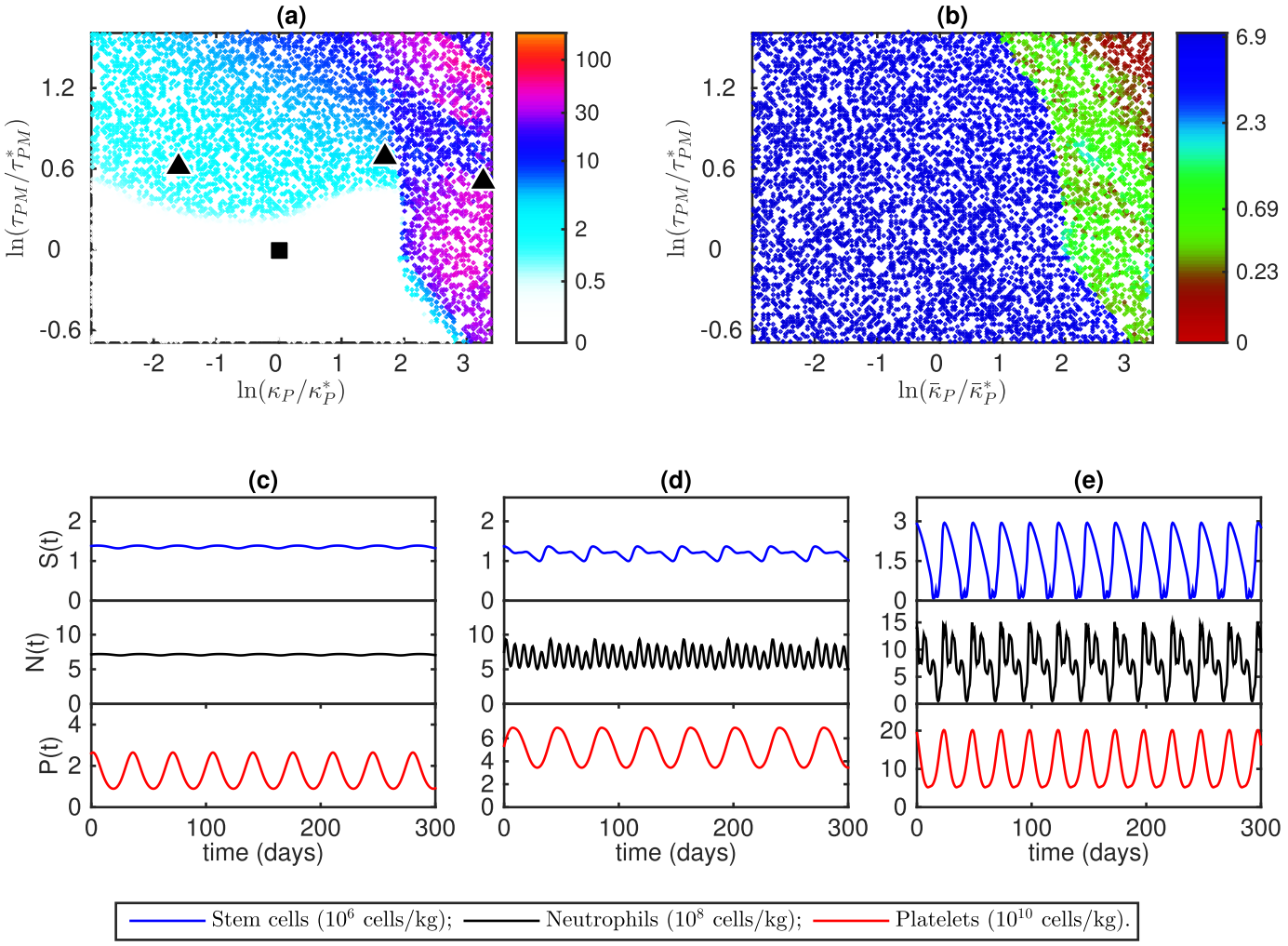

Fig. 2. Simulating hematopoietic dynamics. (a) Dependence of platelet amplitudes on the parameters τ_{PM} and $\bar{\kappa}_P$. The value of the amplitudes are shown by the color, and each dot represents the value for a solution with given parameter values and initial condition from the normal steady state level (other parameters are the same as in Table 1). Parameter values are shown by the logarithm of the ratio to their default values, respectively. The color bar shows the platelet amplitudes (in 10^{10}cells/kg). The black square marks the default parameter value shown. The three triangles mark, from left to right, the location of the parameters corresponding to Pattern 1a, Pattern 1b, and Pattern 2 in Table 2. (b) Dependence of neutrophil nadirs of oscillatory solutions on different parameters τ_{PM} and $\bar{\kappa}_P$. The color bar shows the neutrophil nadir (units of 10^8 cells/kg). (c)–(e) Typical hematopoiesis dynamics with parameters given by black triangles in (a) (from left to right). The bar below (c) through (e) gives the units for the three cell populations. Note that the periods of the neutrophils in (d) and (e) include multimodal periods. Namely, a slow period is present that is the same as in the platelets and HSC, while fast period oscillations are also present that are much shorter than those of the platelets and HSCs.

Table 2
Characteristics and parameters for the three oscillation patters in Fig. 2c–e. Here, we also show some typical oscillation periods.

	Default	Pattern 1a Fig. 2c	Pattern 1b Fig. 2d	Pattern 2 Fig. 2e
Characteristics				
Oscillation in platelets	no	yes	yes	yes
Oscillation in neutrophils	no	no	yes	yes
Nadirs of neutrophils	normal	normal	normal	low
Instances of model parameters and dynamic properties				
$\bar{\kappa}_P$ $(\text{days})^{-1}$	0.372	0.0744	2	9.5442
τ_{PM} (days)	7	13	14	11.583
Period(days)	-	34.8	38.5	24.8

CT-like) and Pattern 1b (unusual CT-like), for the two types of dynamics, respectively (Table 2).

Pattern 2 oscillations showed obviously different dynamics with significant oscillations in all cell lines (Fig. 2e), which is CN-like. In particular, obvious oscillations were observed in the HSC counts, which suggest a destabilization in the stem cell compartment. Moreover, many cases show periods of approximately 20 days, and the neutrophil nadirs are lower than 1/10 of the normal level (Fig. 3a), which are typical in CN. These results suggest that perturbations in the platelet cell line can induce CN-like behavior, which would be a novel mechanism of inducing CN-like oscillations by increasing the platelet differentiation rate $\bar{\kappa}_P$. Here, we mainly focus at the origin of CT. For further discussion of CN dynamics, one can refer to Bernard et al. (2003), Lei and Mackey (2011).

According to the three typical dynamics in Fig. 2, we noted that the oscillations in neutrophil counts were accompanied with oscillations of HSC counts. We compared the relative amplitudes of HSC and neutrophils, which were highly correlated (Fig. 3d). Hence, when dysregulation occurs in the platelet compartment, large amplitude oscillation in HSC often implies significant oscillation in neutrophil counts.

3.2. Comparison with Langlois et al. (2018) patient data

Based on the above analysis of oscillation patterns, we fit our model simulation with patient data from the case report of Langlois et al. (2018). In Langlois et al. (2018), Patient 1 had signif-

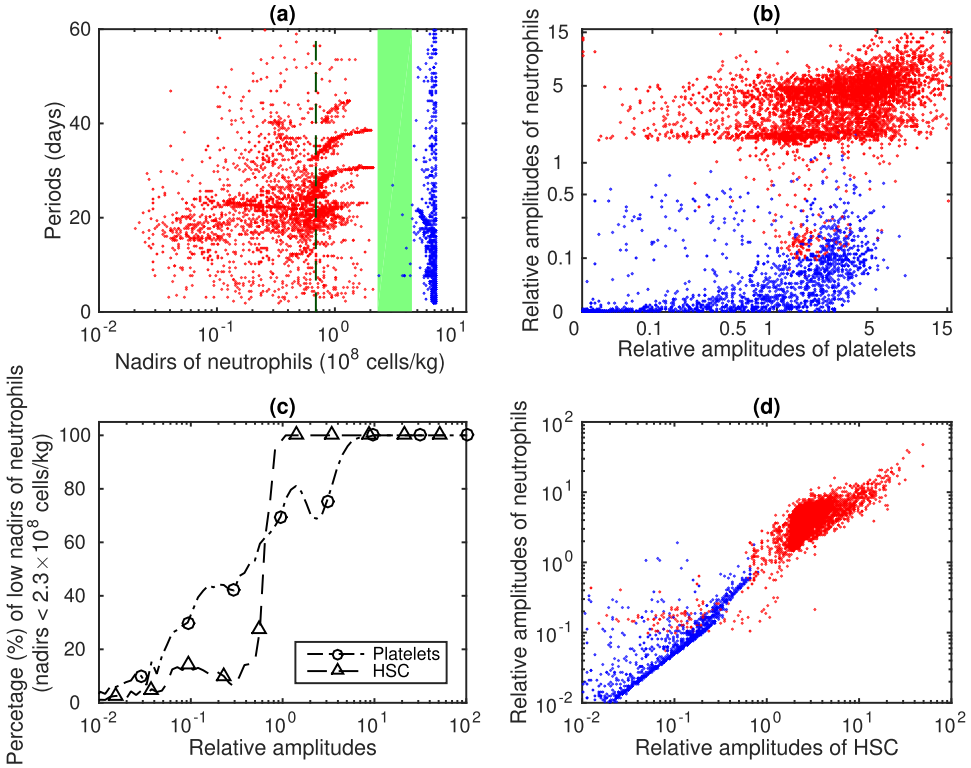

Fig. 3. Characterization of oscillatory dynamics with various parameters $\bar{\kappa}_P$, $\bar{\eta}_P$, τ_{PS}, τ_{PM}, γ_P, ϑ_4, and $A_{P,\max}$ varied from 1/30 to 30 times these default values. All the figures were plotted based on the same set of sampling parameters. (a) Oscillation periods of platelets versus neutrophil nadirs for different sets of parameters. The vertical dashed line shows the nadir of 0.69×10^8 cells/kg, corresponding to 1/10 of the normal level. Blue dots show high nadir neutrophils, and red dots show low level nadirs, which are separated by a gap (green strip) between 2.3 and 4.5 ($\times10^8$ cells/kg). (b) The relative amplitude of neutrophils versus relative amplitude of platelets. Relative amplitudes were calculated by the ratio of the amplitude to the mean level for each oscillatory solution. Colors are the same as in (a). (c) The percentage of parameters with low neutrophil nadir ($<2.3\times10^8$) versus the relative amplitudes of HSC (the triangled line) and platelets (the circled line), respectively. Here, to calculate the percentage, we divided the data set based on the relative amplitudes of platelet or HSC, and calculate the percentage of parameters in a given subgroup to have low neutrophil nadir. (d) The correlation between the relative amplitudes of HSC and neutrophils. Colors are the same as in (a).

Table 3
Parameter values fitting to the clinical data of Langlois et al. (2018) and the key characteristic quantities of the oscillatory dynamics for Patients 1 and 2 in Langlois et al. (2018). The normal values of the parameters from Table 1 are also shown. Note that the changes in $\bar{\kappa}_P$ and τ_{PM} are qualitatively consistent with the changes shown in Table 2 required to produce Pattern 1a (typical CT like) and Pattern 2 (CN like) oscillations, and substantial changes in several other parameters are required in order to achieve precise fits to the clinical data. All units are the same as those in Table 1.

Parameter values to fit to the clinical data.							
	$\bar{\kappa}_P$	$\bar{\eta}_P$	τ_{PS}	τ_{PM}	γ_P	ϑ_4	$A_{P,\max}$
Patient 1	0.102882	106.436	0.547693	18.978	4.92866	9.20914	2057948
Patient 2	0.0872189	0.876661	6.32347	9.26656	0.277219	11.9973	471591
Normal	0.372	0.55	9.5	7.0	0.05	35.9	2^{19}

key quantities							
	Amplitudes of platelets*		Amplitudes of neutrophils*		Periods**	Nadirs of neutrophils	
Cases	clinics	fit	clinics	fit	clinics/fit	clinics	fit
Patient 1	8.09	9.66	4.41	12.5	39 days	2.4	0.58
Patient 2	3.23	4.37	2.49	6.21	23 days	3.17	4.39

* Because of the noise in clinical data, the amplitudes were calculated as follows. 1) divide the dynamics data according to the time window of 90 days. 2) calculate the amplitudes in each time window. 3) averaging over all time windows to get the resulting amplitudes.
** The periods for the fitting data are the same as those in case report (Langlois et al., 2018)

icant oscillations (in the same period) in both platelets and neutrophils, and Patient 2 only displayed significant oscillations in the platelets (Figs. 4 and 5). The fitting parameters and comparison of key quantities for the two patients are shown in Table 3.

For Patient 1, our fitting results are consistent with the clinical data in both amplitude and period of the platelet and neutrophil oscillations (Fig. 4a–d); model simulation reproduces the most significant peak in the spectral power (Fig. 4c–d). In the clinical data, the peak in the neutrophils precedes that in the platelets by 8.3 ± 2.0 days. Our simulation reproduced this phenomenon and the neutrophil peak precedes that of the platelets by 7 days (Fig. 4e). We further predicted the dynamics of TPO by employing the TPO model of Langlois et al. (2017) with the fitted platelet dynamics (i.e., the dynamics shown in Fig. 4a) and HSCs (see Appendix B for details). Our prediction shows that the TPO level oscillates from a nadir of near zero to a maximum of 187 pg/mL, the TPO level is very low during the period of the extremely high level of the platelets count, and vice versa (Fig. 4f), which is qualitatively consistent with the data (Langlois et al., 2018, Fig. 1E).

For Patient 2, model simulations fit to both the amplitude and the period of the reported platelet oscillations well, as well as the neutrophil dynamics (Fig. 5). Furthermore, the predicted spectral

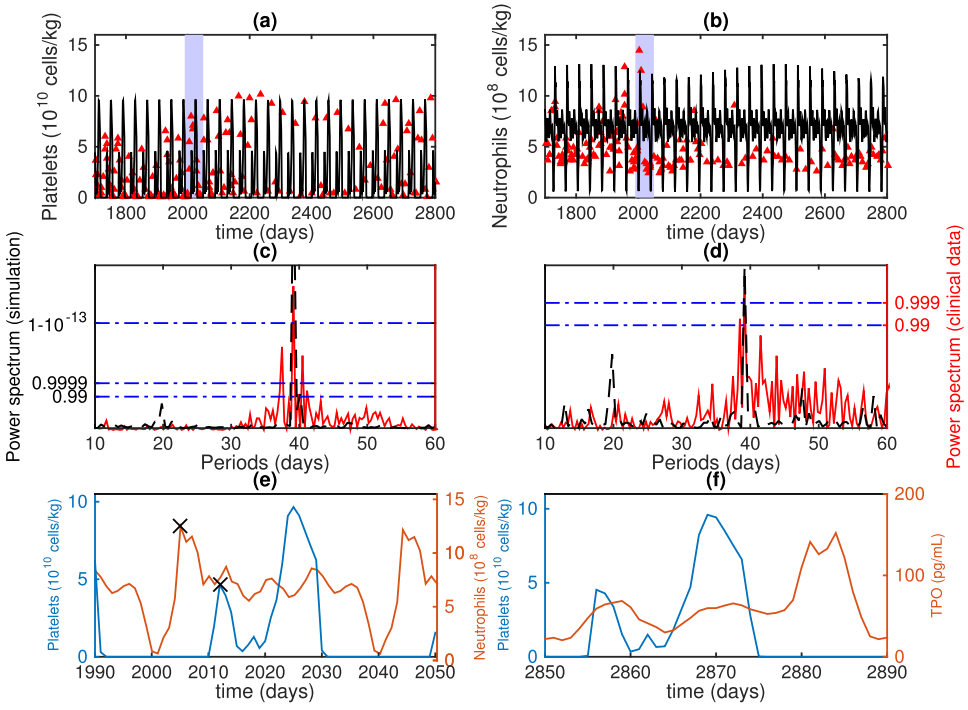

Fig. 4. Fitting the clinical data of Langlois et al. (2018, Patient 1). The fitting parameters are shown in Table 3, and the time is appropriately shifted to fit the data. (a) Platelet count dynamics. (b) The dynamics of neutrophil counts. In both panels, red triangles denote clinical data, and black solid lines are the model simulation. (c) The spectral power of the platelet dynamics. Horizontal dashed-dotted lines indicate the statistical significance levels of oscillations (Lomb, 1976). (d) The spectral power of neutrophil dynamics. Red lines are for the patient data and dashed black lines are the spectral power of simulation dynamics. (e) A period of simulated dynamics of both platelets and neutrophils. The two crosses show the first peaks from the nadirs in neutrophils and platelets, which occur at days 2029 and 2036, respectively. (f) Simulated dynamics of platelets and TPO (see Appendix B for details of the TPO simulation).

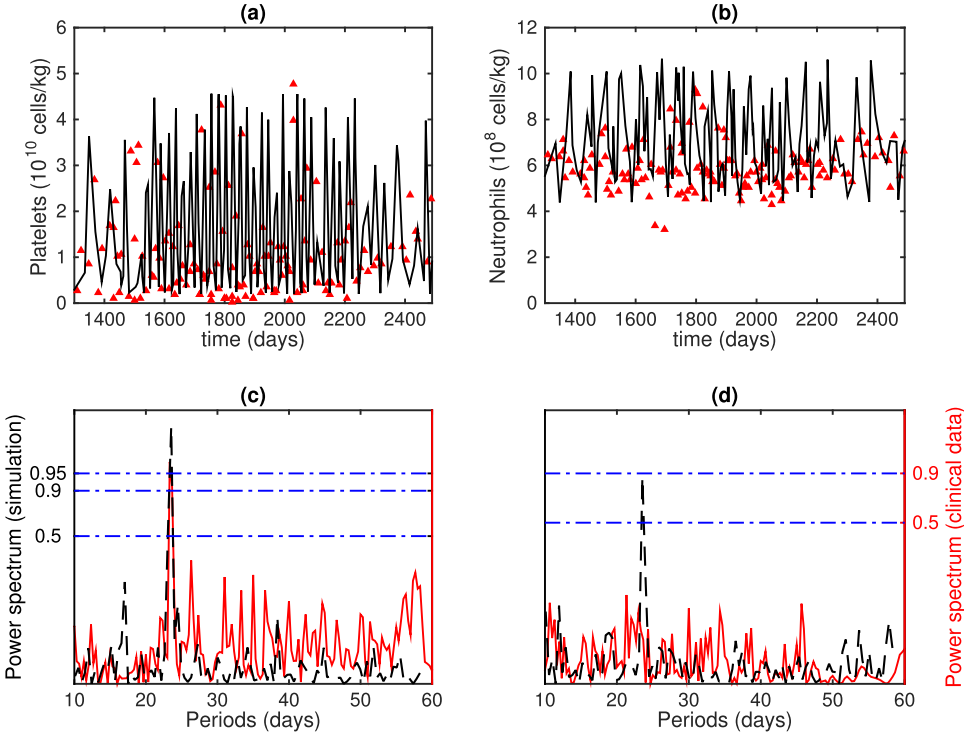

Fig. 5. Fitting the clinical data of Patient 2 in the case report Langlois et al. (2018). (a) The dynamics of platelet counts. (b) The dynamics of neutrophil counts. Red triangles are clinical data, and black solid lines are model simulation. (c) The spectral power of the platelet dynamics. (d) The spectral power of neutrophil dynamics. Red lines are the spectral power of the clinical data and dashed black lines are the spectral power of simulation dynamics. Refer to Table 3 for parameters.

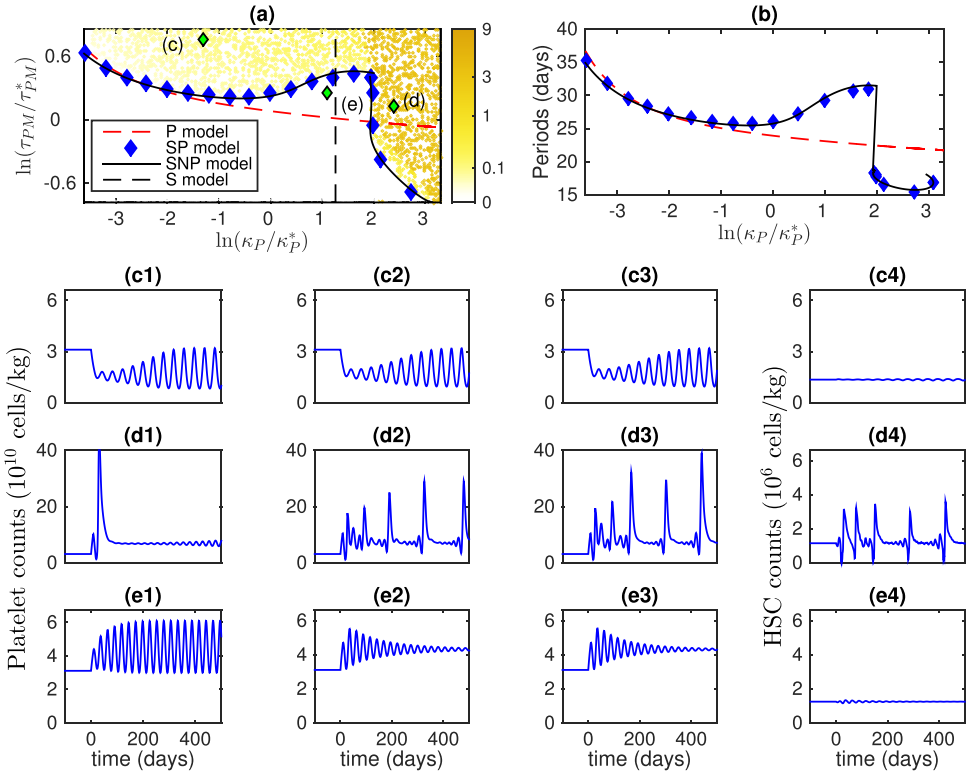

Fig. 6. Bifurcation diagram of the model equations. (a) Numerical bifurcation curves of different models and amplitudes of HSC counts in the *SNP* model. The bifurcation curves are obtained based on the *SNP* model (solid black line), *SP* model (blue dots), *P* model (red dashed line), and the *S* model (black dashed line). Points c-f mark the parameters with corresponding platelet dynamics shown at panels (c)–(e), respectively. The yellow dots in background represent the amplitudes of the HSC counts by means of shades of the colors as shown in the colorbar. The units of the amplitudes of HSC are 10^6 cells/kg. (b) Periods at the Hopf bifurcation point. The periods are calculated based on the linear stability. The meanings of lines are the same as those in (a). (c1)–(c3) Time evolution of platelets when the parameters are at c in (a). Here (c1) for the P model, (c2) for the *SP* model, and (c3) for the *SNP* model. (c4) is the time course of the dynamics of stem cell counts of the *S* model (13). (d1)–(d4) Same as (c1–4), with parameters taken at point d in (a). (e1)–(e4) Same as (c1–c4), with parameters taken at point e in (a).

power is consistent with that from the clinical data with the most significant peak in the spectral power of the platelet dynamics at 23.5 days in simulations, agreeing well with that of the clinical data (23.3 days) (Fig. 5c). For the spectrum of neutrophils, the significance level for the principal peaks obtained from simulation is less than 0.9 (Fig. 5d); hence, the oscillations in the neutrophil counts were not significant, which is qualitatively consistent with the clinical data. Here, we note that the spectrum of the fitting dynamics was more significant than that for the clinical data. This difference may come from random fluctuations in clinical data that can counteract the small amplitude oscillations.

3.3. Numerical bifurcation analysis

In previous simulations, we had noted that varying the parameters $\bar{\kappa}_P$ and τ_{PM} can results in obvious oscillations either only in platelet counts or in all cell lines. Here, we further apply numerical bifurcation analysis to investigate the sources of various oscillation patterns.

The bifurcation curve of the *SNP* model is shown as the solid line in Fig. 6a. Given the constant initial condition at their normal steady states, the system shows oscillatory dynamics when τ_{PM} is larger than the corresponding point on the bifurcation curve and the system converge to a stable steady state when τ_{PM} is smaller. Fig. 6b shows the periods of oscillatory solutions, which was when the parameters were taken near the bifurcation curve.

To further understand and analyze the core origin of these oscillation patterns, inspired by the close relation between the relative amplitudes of HSC counts and neutrophil counts (Fig. 3c), we omitted the feedback from the neutrophil compartment and considered the *SP* model (11) and (12) for the dynamics of the HSC and platelet compartments.

The numerically determined bifurcation points are shown by blue diamonds in Fig. 6a, which indicate the parameters $(\bar{\kappa}_P, \tau_{PM})$ at which the steady state becomes unstable. Fig. 6b shows the oscillation periods when parameters were taken from the bifurcation curves. From Fig. 6a and b, the bifurcation curve as well as the periods obtained from the reduced *SP* model, agrees well with the curve obtained from the *SNP* model. These results indicate that the dynamic properties of the *SNP* model in platelet counts are maintained without the feedback from the neutrophil compartment. Moreover, we have seen that the relative amplitudes between the HSC and neutrophils are closely related (Fig. 3c), which implies that the neutrophil oscillation patterns can be derived from the HSC dynamics. Consequently, the above analysis showed that the dynamics based on regulation in the HSC and platelet cell lines alone are sufficient to reveal the origin of the CT-like oscillations: namely, that the dysregulation in the HSC and platelet dynamics is apparently sufficient to generate the CT-like oscillations as well as the platelet-originated CN-like oscillations.

From Fig. 6a, the oscillatory dynamics can be induced by at least two different approaches. The first one is the increase in the megakaryocyte maturation time τ_{PM}, when the maximum differentiation rate $\bar{\kappa}_P$ is small. In this case, the amplitudes of the HSC counts are essentially close to zero (light yellow points on the left top areas in Fig. 6a). Second, the oscillation can also be induced by increasing the maximum differentiation rate $\bar{\kappa}_P$, where the amplitudes of HSC counts are significantly larger (Fig. 6a).

These observations led us to further explore the origin of oscillations with changes in the two parameters τ_{PM} and $\bar{\kappa}_P$. To this

end, we considered the reduced *S* and *P* models ((13) and (14)) to investigate the roles of dysregulation in the HSC and platelet compartments.

Previous studies based on a bifurcation analysis for the *S* model have shown that oscillations in the HSC counts emerge when the differentiation rate κ increases above a threshold (Ma et al., 2015) (Fig. 6a, black dashed line) and the role of the maturation time in the *S* model have been analyzed (Câmara De Souza et al., 2018). The numerical bifurcation analysis for the *P* model shows that the bifurcation is mainly determined by the megakaryocyte maturation time τ_{PM} (Fig. 6a, red dashed line).

As shown in Fig. 6a, when the differentiation rate $\bar{\kappa}_P$ is small, the values of τ_{PM} where bifurcation appears for the three models (*SNP*, *SP*, and *P*) are similar. In these cases, alterations in the *P* model alone can induce oscillations by destabilization of the platelet cell line through increasing the megakaryocyte maturation time τ_{PM}. In addition, the amplitudes of the neutrophils and HSCs are small, and the neutrophil and HSC counts vary around their steady states. Hence, the platelet oscillations in the *SNP* or *SP* models are mainly due to alteration in the platelet cell line, and the oscillation dynamics in the platelet cell line do not significantly affect the dynamics of neutrophils or HSCs. These results suggest a mechanism of CT generation through the destabilization of the platelet cell line by increasing the megakaryocyte maturation time τ_{PM}.

We took a parameter (point c in Fig. 6a) with a small value of $\bar{\kappa}_P$ and solved the equations of the *P*, *SP*, and *SNP* models with the initial conditions of the constant steady state platelet counts. Solutions based on the three models show similar oscillation patterns in the platelet counts (Fig. 6, c1–c3), whereas the HSC dynamics obtained from the *S* model remained near the stable steady state (Fig. 6, c4). Hence, when the differentiation rate is small, the platelet count dynamics seem to be mainly determined by the regulation in the platelet cell line.

On the other hand, when the differentiation rate $\bar{\kappa}_P$ is large, the HSC oscillates significantly with large amplitudes. From Fig. 2a, the amplitudes of the platelets in this area are much larger than those in the region of the smaller $\bar{\kappa}_P$. These two facts suggest that a large amplitude in platelet oscillations may induce the unstable dynamics of HSC and result in the oscillatory dynamics in all cell lines; consequently, the system displays Pattern 2 (CN-like) oscillations. An example is shown in Fig. 6 (d1–d4) with parameter values given by point d in Fig. 6a. The platelet amplitudes in the *SP* model and the *SNP* model are much larger than those in the *P* model. In addition, in this region, the bifurcation point τ_{PM} for the *P* model is larger than that for the *SP* and *SNP* models. These observations suggest that in the large $\bar{\kappa}_P$ region, platelet-induced unstable HSC counts enhance the oscillation of the platelet counts.

At the transition region with the intermediate value $\bar{\kappa}_P$ and when the maturation time τ_{PM} is larger than the bifurcation value for the *P* model (point e in Fig. 6a), the normal steady state is unstable in the *P* model but is stable in the *SP* and *SNP* models (Fig. 6, e1–e3). Moreover, we note the essentially negligible amplitude of the HSC counts in this region (compare Fig. 6e4 with Fig. 6d4). Hence, for parameters in this region, the amplitudes of platelets are smaller than those for large $\bar{\kappa}_P$, and the negative feedback to the differentiation rate is able to weaken the oscillations induced by platelets. These results indicate that coupling of the HSC compartment to the platelet cell line can serve as a pool to stabilize small perturbations in the platelet counts induced by increasing the maturation time τ_{PM}.

Previous studies have shown that bistability with coexistence of both a stable steady state and an oscillatory state can emerge based on a mathematical model of HSC and neutrophil dynamics (Bernard et al., 2003; Ma et al., 2015). In the present model, bistability is observed when we set parameters $\bar{\kappa}_P$ and τ_{PM} at the point e in Fig. 6a and $\gamma_P = 0.15$, $\bar{\eta}_P = 0.1$. We solved the equations with oscillatory or constant platelet levels as initial conditions, whereas other cell lines were taken at their normal steady states (Fig. 7, a–c). The results show bistability in both *SNP* and *SP* models. Solutions with constant initial platelet counts converge to constant levels (blue lines in (b)–(d)), but solutions with oscillatory initial conditions converge to the stable oscillatory solutions (red line in (b)–(d)). These results show that the long-term behavior of the *SP* or *SNP* models may show sensitivity in its dependence on the parameter values as well as on the initial conditions. This result is similar to those for CN (Lei and Mackey, 2011). For systems with bistability, one cannot take the system back to a normal state simply by changing the parameters back to their normal values but must also control the states of all cell lines.

Moreover, we sampled the parameter space to obtain the area for $\bar{\kappa}_P$ and τ_{PM} (Fig. 7d, the black dots) within which the *SP* and *SNP* models show bistability with a proper choice of γ_P and $\bar{\eta}_P$, and initial oscillatory conditions generate oscillatory solutions. We also found that, outside the visible region in Fig. 7d, parameters exists for which the system shows bistability, and constant initial conditions do not necessarily imply a stable steady state. For example, when we took $(\bar{\kappa}_P, \tau_{PM})$ as $\bar{\kappa}_P = 4.5$, $\tau_{PM} = 90$ and $\gamma_P = 0.22$, $\bar{\eta}_P = 0.11$, the system dynamics evolves to stable steady states from initially oscillatory condition, whereas the constant initial conditions can result in oscillatory dynamics (Fig. 7e). For this specific sample, oscillatory initial conditions in the platelet compartment result in the very low counts in HSC, and in turn, make the counts of platelets eventually drop to low levels. Previous discussion has shown that in the bistable region below the bifurcation curve, the HSC compartment acts as a stabilizer of the system. In this region, the opposing effects of HSC and platelets on the system may contribute to the bistability and for extreme abnormal differentiation rate and maturation time, the bistability pattern (zero and oscillations) is suggested to be different from those in the region around the default values (positive steady states and oscillations). This transition as a further mechanism for the occurrence of bistability is beyond the scope of the current study.

4. Conclusion and discussion

In this study, we examined the dynamics of hematopoiesis regulation using a simplified model for the HSC, the platelets and the neutrophils. Our aim was to try to understand the nature of the clinical situation in a cyclical thrombocytopenia patient reported by Langlois et al. (2018); this patient showed concomitant neutrophil and platelet oscillations with no signs of a mutation characteristic of cyclical neutropenia. Cyclical thrombocytopenia is normally characterized by significant oscillations in platelet counts without oscillations in the neutrophils.

Through the examination of system response to regulation in the platelet compartment, by varying the differentiation rate $\bar{\kappa}_P$ and the maturation time τ_{PM}, we identified the conditions needed to induce oscillations only in platelet counts while the neutrophil population varied around its normal levels with small fluctuations (Pattern 1a oscillations), and oscillations in both platelet and neutrophil counts (Pattern 1b oscillations). In additional to cyclical thrombocytopenia, we also identified parameters that yield cyclical neutropenia-like dynamics (Pattern 2), which showed significant oscillations in both platelet and neutrophil numbers. These results explain the recent case report that cyclical thrombocytopenia patients can also display oscillations in the neutrophils (Langlois et al., 2018), and raises the possibility of inducing cyclical neutropenia-like symptoms due to defects in the platelet compartment alone.

Numerical bifurcation analysis based on the differentiation rate $\bar{\kappa}_P$ and maturation time τ_{PM} has shown two possible origins of

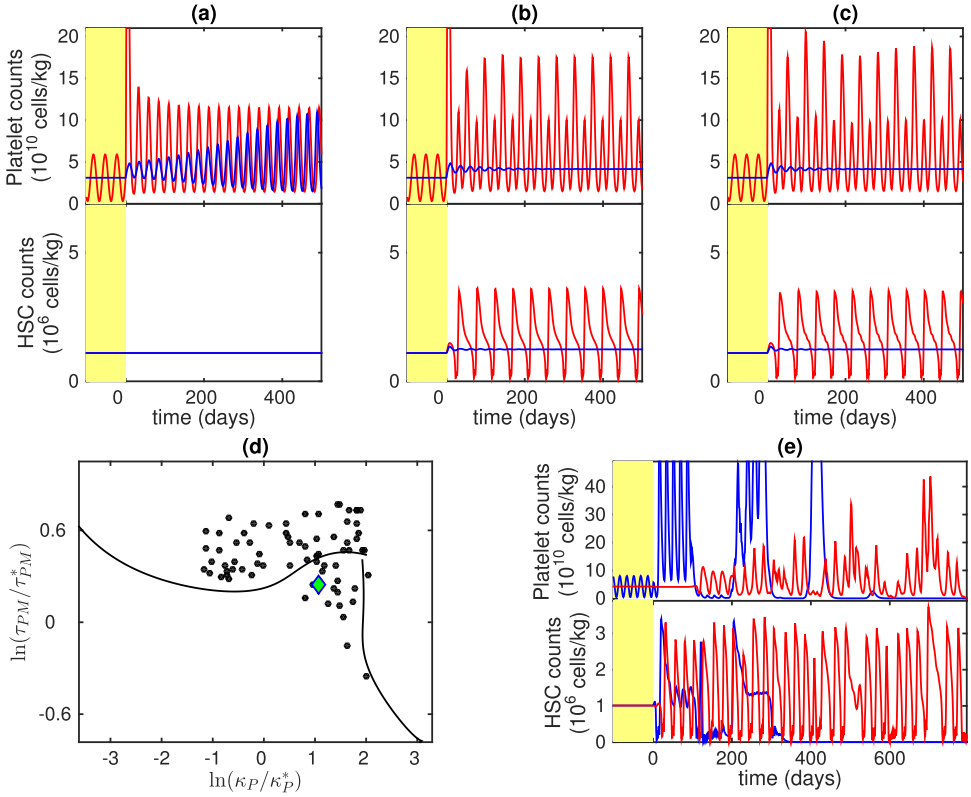

Fig. 7. Bistability of the model equations. (a)-(c) Dynamics with different initial conditions of the *P*, *SP*, and *SNP* models respectively. $\bar{\kappa}_P$ and τ_{PM} are taken as the green diamond point in (d) (i.e. the point **e** in Fig. 6(a)) and $\gamma_P = 0.15$, $\bar{\eta}_P = 0.1$. (a)-(c) Blue lines were obtained from solutions with constant platelet counts initial conditions, and red lines were obtained from solutions with oscillatory platelet count initial conditions. Initial conditions for the other cell lines remain constant at their normal steady states. (d) The dots are the values of $\bar{\kappa}_P$ and τ_{PM} at which bistability is observed with suitable γ_P and $\bar{\eta}_P$ values. The solid line is the bifurcation curve of the *SNP* model as in Fig. 6a. The green diamond point shows the values of $\bar{\kappa}_P$ and τ_{PM} used for (a)–(c) (same as point **e** in Fig. 6a). (e) The dynamics of the *SNP* model where the constant initial conditions induce oscillations while the oscillatory initial conditions induce stable steady states. The parameters are taken as $\bar{\kappa}_P = 4.5$ (i.e., $\ln(\bar{\kappa}_P/\bar{\kappa}^*_P) = 2.49294$), $\tau_{PM} = 90$ (i.e., $\ln(\tau_{PM}/\tau^*_{PM}) = 2.5539$), $\gamma_P = 0.22$, $\bar{\eta}_P = 0.11$.

platelet oscillation. The first one is from the destabilization of the platelet compartment through the increasing of maturation time τ_{PM}. The second is the destabilization of the HSC compartment due to the upregulation of the differentiation rate. The two sources induce cyclical thrombocytopenia-like oscillation and cyclical neutropenia-like oscillations, respectively. Other sources of the oscillations and patterns remain for further investigation.

Our study theoretically uncovers a possible mechanism of cyclical thrombocytopenia through the perturbation in the platelet compartment, and suggests a possible connection between cyclical thrombocytopenia and cyclical neutropenia. These results may stimulate further experimental and/or clinical verification. Although we have been able to obtain a fit to the data in Langlois et al. (2018) for the two patients displaying dramatically different oscillatory patterns, this was achieved with large changes in seven different parameters, which indicates we have likely not captured the essence of platelet and neutrophil regulation with this model. This study provides a qualitative explanation of the connections between cyclical thrombocytopenia and cyclical neutropenia. However this new mechanism and more comprehensive dynamical responses in the hematopoietic system await further investigation.

Acknowledgement

This work was supported by National Natural Science Foundation of China (NSFC 11626040 and 11801020), the Foundation for Connotation Development of Beijing University of Technology (107000514116003, 107000514117001), Fundamental Research Funding of Beijing University of Technology (006000546318505), and the Natural Sciences and Engineering Research Council of Canada. We would like to especially thank Gabriel P. Langlois for providing the patient data from Langlois et al. (2018) to us, and Prof. Humphries (McGill) for most helpful comments on an early version of this paper.

Appendix A. Parameters in the platelet compartment

Most model parameters in the HSC and neutrophil compartments were taken from Colijn and Mackey (2005a) and Zhuge et al. (2012), and most parameters in the platelet compartment were from Lei and Mackey (2011). Other parameters were calculated or assumed based on existing models so that in the normal system the three blood cell levels are stable at their normal value.

For parameters in the platelet compartment, we took the default level of platelets P_* and the apoptosis rate of circulating platelet γ_P as in Langlois et al. (2017) so that our model matches their model for these two parameters. We also set the differentiation rate at the default platelet level as that used in Langlois' model, so

$$\kappa^*_P = 0.0072419 \text{ day}^{-1}.$$

The maturation time τ_{PM}, the maximal life time of platelets τ_{PS}, the parameters K_P, and the s_4 that appear in the differentiation rate of platelets κ_P (Eq. (3)) were taken from Colijn and Mackey (2005a) and Lei and Mackey (2011). Thus, we obtained the

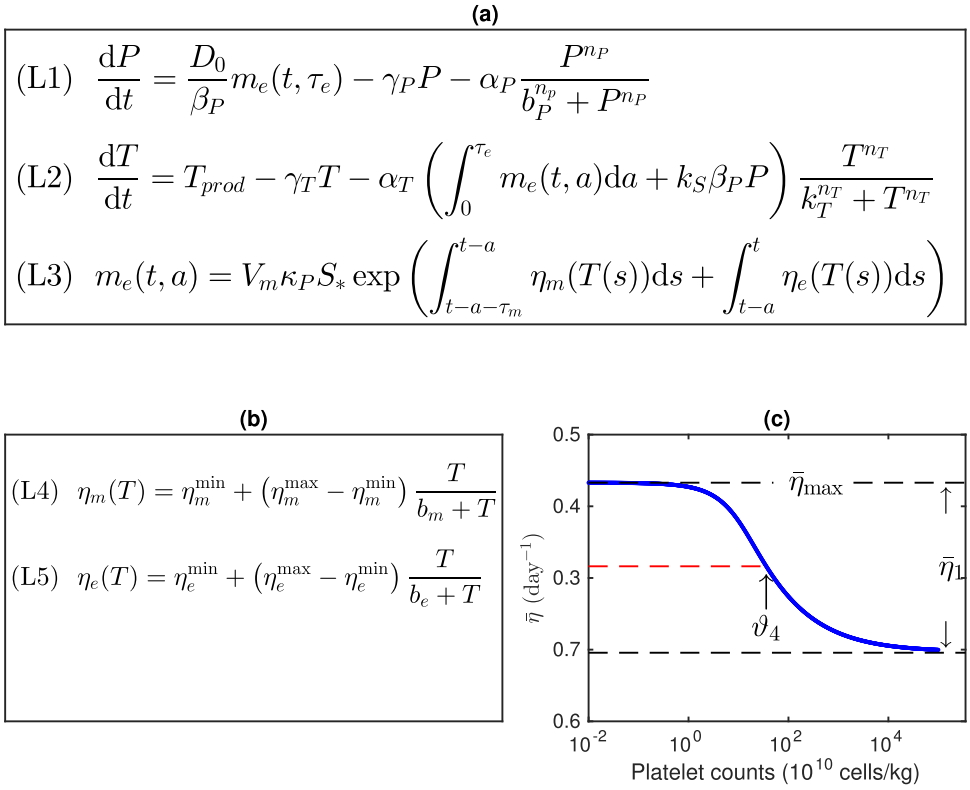

Fig. 8. The model equations and numerical results of Langlois et al. (2017). (a) The model equations in Langlois et al. (2017) that govern the dynamics of platelet counts (P), TPO level (T) and the volumes of megakaryocytes of age a ($m_e(t, a)$). (b) The functions describing the proliferation rates of megakaryoblasts (η_m) and megakaryocytes (η_e). (c) The dependence of $\bar{\eta}$ on platelet counts P in Langlois et al. (2017). The blue solid line shows the relation of platelet counts and $\bar{\eta}$ defined in (16) at steady states. The red dashed line shows the average of the maximum and minimum of $\bar{\eta}$, and the x coordinate of the uparrow indicates ϑ_4. The quantities $\bar{\eta}_{\max}$ and $\bar{\eta}_1$ are shown by corresponding markers.

value of $\bar{\kappa}_P$ as follows.

$$\bar{\kappa}_P = \kappa_P^* \left(K_P P_*^{s_4} + 1\right) = 0.0072419\left(1 + 11.66 \times 3.1071^{1.29}\right) = 0.372 \text{ day}^{-1}.$$

The parameters in the proliferation A_P and apoptosis of platelet precursors η_P, which appear in the functions (5) and (7), were calculated based on fitting of numerical results in Langlois et al. (2017). In the Langlois model, the dynamics of the platelet counts are governed by the equations shown in Fig. 8(a) and (b). The platelet precursors are regulated by a negative feedback loop involving thrombopoietin (TPO) and platelets.

To obtain the relation between the amplification factor A_P and the platelet level P, we calculated the effective proliferation rate $\bar{\eta}$ through the TPO dynamics in the Langlois model and then translated $\bar{\eta}$ to A_P in our model. Therefore, a comparison of Eqs. (8)–(10) with the Langlois model is reasonable. The logarithm of the amplification factor A_P in our model is proportional to the effective proliferation rate $\bar{\eta}$ in the Langlois model (Fig. 8)

$$\ln A_P \propto \bar{\eta} := \frac{1}{\tau_e + \tau_m} \left(\int_{\tau_e}^{\tau_e + \tau_m} \eta_m(T(t-a))da + \int_0^{\tau_e} \eta_e(T(t-a))da \right). \tag{15}$$

Next, we solved for the steady states of thrombopoietin T with different levels of platelets P through equation (L2) in Fig. 8a to obtain the dependence of $\bar{\eta}$ on the levels of platelets P (Fig. 8c). As shown in Fig. 8c, the dependence of $\bar{\eta}$ on P is a Hill function

$$\bar{\eta} = \bar{\eta}(P) = \bar{\eta}_{\max} - \bar{\eta}_1 \frac{P^{\nu_4}}{\vartheta_4^{\nu_4} + P^{\nu_4}}, \tag{16}$$

where $\bar{\eta}_{\max}$ is the maximum of $\bar{\eta}$, $\bar{\eta}_1$ is the difference between maximum and minimum of $\bar{\eta}$, and ϑ_4 is the level of platelets such that $\bar{\eta}$ is at the average of its maximal and minimal values (Fig. 8a). Hence, we were able to determine the parameters in (16) as follows.

$$\bar{\eta}_{\max} = 0.6329 \text{ day}^{-1},\ \bar{\eta}_1 = 0.2372 \text{ day}^{-1},\ \vartheta_4 = 35.9 \times 10^{10} \text{ cells/kg}.$$

$A_{P,\max}$ in our model can be represented in terms of the parameters in the Langlois model as follows.

$$\begin{aligned} A_{P,\max} &= \frac{D_0 V_m}{\beta_P} \exp\left[\bar{\eta}_{\max}(\tau_e + \tau_m)\right] \\ &= \frac{0.21829}{8.6} \frac{4\pi \times 21^3}{24} e^{0.632918 \times (5+8.09)} = 487837. \end{aligned}$$

For the Hill coefficient ν_4, from Eq. (7), we have

$$\nu_4 = \frac{\ln\left(\frac{\bar{\eta}_1}{\bar{\eta}_{\max} - \bar{\eta}} - 1\right)}{\ln(\vartheta_4 / P)}.$$

Therefore, we obtained the value of ν_4 by taking the average of each pair of numerical values of platelet levels and the values of $\bar{\eta}$ as shown in Fig. 8. We have

$$\nu_4 = 1.00. \tag{17}$$

Next, we calculated the parameters in Eq. (7). To do this, we calculated the normal amplification factor as follows.

$$\begin{aligned} A_P^* &= \frac{D_0 V_m}{\beta_P} \exp(\bar{\eta}(P_*)(\tau_e + \tau_m)) \\ &= \frac{0.21829}{8.6} \frac{4\pi 21^3}{24} e^{0.614852 \times (5+8.09)} = 385100. \end{aligned}$$

So, from Eq. (5), we have

$$\begin{aligned}\bar{\eta}_P &= \frac{1}{\tau_{PM}} \ln\left(\frac{A_{P,\max}}{A_P^*}\right)\frac{\vartheta_4^{\nu_4}+P_*^{\nu_4}}{P_*^{\nu_4}}\\ &= \frac{1}{7}\ln\left(\frac{487837}{385100}\right)\frac{35.9+3.1071}{3.1071}\\ &= 0.424 \text{ day}^{-1}.\end{aligned}$$

The differentiation rate κ_R^* was given by the normal differentiation rate in Colijn and Mackey (2005a):

$$\kappa_R^* = \frac{\bar{\kappa}_r}{1+K_r R_*^6.96} = \frac{1.1}{1+0.0382\times 3.5^{6.96}} = 0.00469 \text{ days}^{-1}.$$

Finally, we estimated the parameters in the neutrophil compartment. We set the parameters in the neutrophil compartment based on Colijn and Mackey (2005a) and Zhuge et al. (2012), except for the apoptosis rate of precursors η_N, because our formulation of the neutrophil compartment dynamics was identical with those two models with the only exception being in the apoptosis of precursors.

Since we have introduced the apoptosis of precursors into our model, the parameter $A_{N,\max}$ was calculated with the normal amplification factor being calculated from Eq. (1) in Zhuge et al. (2012), which gives $\bar{\eta}_N = 0.27$ day^{-1} and $A_N^* = \exp(2.5420\times 5 - 0.27\times 6) = 65512.7$.

Now, we assume that the apoptosis of the precursors of neutrophils follows a similar pattern as in the platelets. We simply assumed that $\frac{\vartheta_4}{P_*} = \frac{\vartheta_1}{N_*}$ and $\nu_1 = \nu_4$. Thus,

$$\vartheta_1 = \frac{\vartheta_4 N_*}{P_*} = 79.7\times 10^8 \text{ cells/kg}, \quad \nu_1 = 1.$$

Finally, the maximal amplification factor of the neutrophil precursors was estimated to obtain as follows.

$$A_{N,\max} = A_N^* \exp\left(\bar{\eta}_N \frac{N_*^{\nu_1}}{\vartheta_1^{\nu_1}+N_*^{\nu_1}}\tau_{NM}\right) = 70635.$$

Appendix B. Predicting the TPO dynamics from model simulation

The model in the current study does not include TPO dynamics explicitly. To obtain a prediction of TPO dynamics from platelets and HSC counts, we used TPO dynamical equations shown by (L2) in Fig. 8. Since $P(t)$ and $S(t)$ come from the SNP model, equation (L3) was replaced with

$$\begin{aligned}(\text{L3}') \quad m_e(t,a) &= V_m \kappa_P(P(t))S(t)\\ &\times \exp\left(\int_{t-a-\tau_m}^{t-a}\eta_m(T(s))\text{d}s + \int_{t-a}^{t}\eta_e(T(s))\text{d}s\right).\end{aligned}$$

Here $\eta_m(T)$ and $\eta_e(T)$ are defined by (L4) and (L5) in Fig. 8. All parameters not appearing in our SNP models (8)–(10), except τ_e and τ_m, which were taken from Langlois et al. (2017). We took values for τ_e and τ_m so that they satisfy $\tau_e+\tau_m = \tau_{PM} = 18.978$ days and the ratio τ_e/τ_m is the same as in Langlois et al. (2017). The fitting simulation result, based on the fitting parameters for Patient 1 in Langlois et al. (2018), is shown at Fig. 4f.

Appendix C. Comparison between the dynamics of the SNP model and the SNP model with erythrocyte compartment

In this study, the effects of the erythrocyte compartment were simplified as a single differentiation rate κ_R^*. To justify the validity of this simplification, we can add the erythrocyte compartment to the *SNP* model (8)–(10) based on the models of Colijn and Mackey (2005a), and compare the dynamics obtained from the two models. The modified model equations are given below (18)–(21).

$$\begin{aligned}\frac{dS}{dt} &= -(\beta(S)+\kappa_N(N)+\kappa_P(P)+\kappa_R(R))S\\ &\quad + 2e^{-\gamma_S\tau_S}\beta(S_{\tau_S})S_{\tau_S}\end{aligned} \tag{18}$$

$$SNRP\ Model: \quad \frac{dN}{dt} = -\gamma_N N + A_N(N_{\tau_{NM}})\kappa_N(N_{\tau_{NM}})S_{\tau_{NM}} \tag{19}$$

$$\begin{aligned}\frac{dR}{dt} &= -\gamma_R R + A_R\big(\kappa_R(R_{\tau_{RM}})S_{\tau_{RM}}\\ &\quad - e^{-\gamma_R\tau_{RS}}\kappa_R(R_{\tau_{RSum}})S_{\tau_{RSum}}\big)\end{aligned} \tag{20}$$

$$\begin{aligned}\frac{dP}{dt} &= -\gamma_P P + A_P(P_{\tau_{PM}})\big(\kappa_P(P_{\tau_{PM}})S_{\tau_{PM}}\\ &\quad - e^{-\gamma_P\tau_{PS}}\kappa_P(P_{\tau_{PSum}})S_{\tau_{PSum}}\big),\end{aligned} \tag{21}$$

where

$$\kappa_R(R) = \frac{\bar{\kappa}_R}{1+K_r R^{s_3}}.$$

The model formation and parameters were based on Colijn and Mackey (2005a). The parameters for the red blood cell compartment were taken as Colijn and Mackey (2005a): $\gamma_R = 0.001, \bar{\kappa}_R = 1.1, A_R = 563000, K_r = 0.0382, s_3 = 6.96, \tau_{RM} = 6, \tau_{RS} = 114, \tau_{Rsum} = \tau_{RM}+\tau_{RS}$.

The comparison is shown in Fig. 9. We compared the dynamical trajectories of Patterns 1a, 1b and 2 (See Fig. 2(c)–(e)). The blue solid lines represent the dynamics according to the *SNP* model and the pink marked dotted lines represent the simulations by *SNRP* models. The *SNP* and *SNRP* models are consistent for Patterns 1a and 1b (Fig. 9(a)–(b)) and for Pattern 2 (Fig. 9), although the oscillation phases are different in platelet compartment, the amplitudes and periods are mostly consistent to each other within the two models. To further verify our simplification, we compared the amplitudes and periods of the platelet dynamics with random choices of all seven parameters as in Section 3.1 (Fig. 9d). The amplitudes and periods obtained from the two models are closely correlated. Hence, our simplification of neglecting the erythrocyte compartment does not affect the results in our study.

Appendix D. Procedures to obtain the fitting parameters for Langlois et al. (2017) patient data

In fitting the data, we were not trying to fit each discrete data point. Instead, we applied the following procedure based on a genetic algorithm to identify parameters to fit the characteristic measurements of oscillation dynamics in the clinical data.

First, we set the following optimization problem

$$\begin{aligned}\min \ &\sum_{i=P,N}\Big(\big|\text{amp}_{i,sim}-\text{amp}_{i,cli}\big| + \big|\text{nadir}_{i,sim}-\text{nadir}_{i,cli}\big|\\ &+3\big|\text{period}_{i,sim}-\text{period}_{i,cli}\big|\Big)\\ &+\sum_{i=P,N}\text{average}_f\left|\frac{\text{spectra}_{i,sim}(f)-\text{spectra}_{i,cli}(f)}{\max_f \text{spectra}_{i,cli}(f)}\right|,\end{aligned} \tag{22}$$

where $\text{amp}_{i,j}$ represent the amplitudes of platelets ($i=P$) or neutrophils ($i=N$) in the simulated dynamics ($j=sim$) or the clinical data ($j=cli$); $\text{period}_{i,j}$ and $\text{nadir}_{i,j}$ represent the periods and nadirs, respectively, with i and j having the same meaning as those of $\text{amp}_{i,j}$; and $\text{spectra}_{i,j}(f)$ is the spectral power at the frequency f with i and j as before.

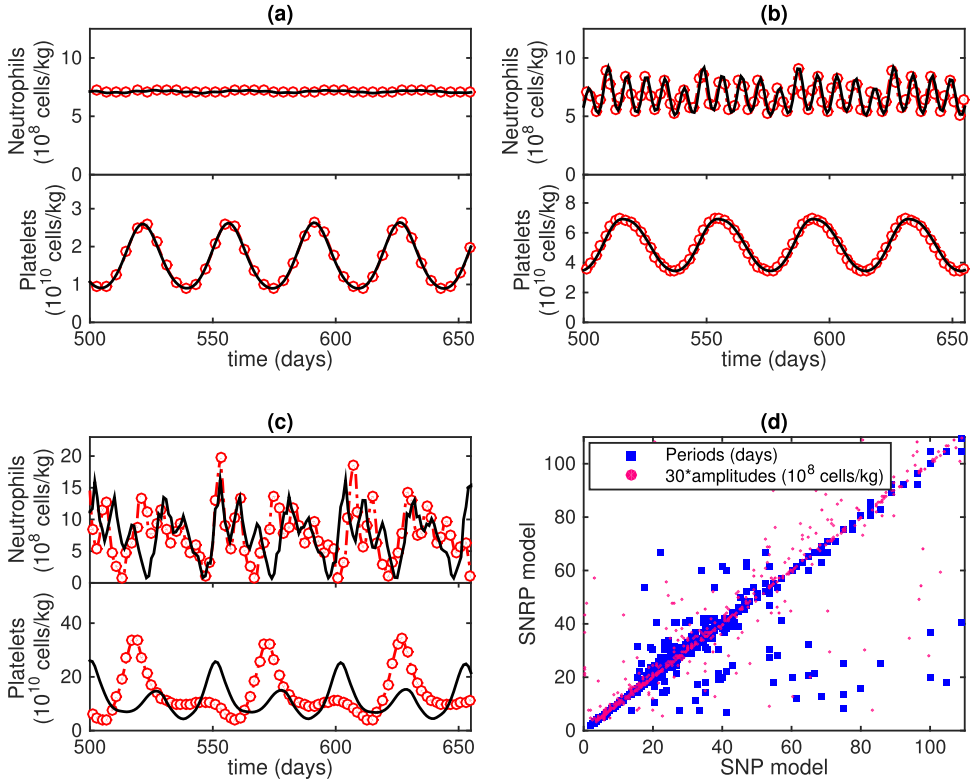

Fig. 9. The comparison between the *SNP* model and the *SNRP* model. (a)–(c) The dynamics of platelets and HSC in *SNP* and *SNRP* models with parameters taken for Pattern 1a, 1b and Pattern 2, respectively. Black solid lines represent the dynamics in *SNP* model and the red dotted marked lines represent the dynamics of *SNRP* model. (d) Comparison of amplitudes and periods with randomly chosen parameters. Pink squares for amplitudes, and blue for periods. Here, we have rescaled the amplitude and period values to make the values consistent with each other.

Second, we started with a randomly chosen set of parameters drawn from the parameters that generate Fig. 3 and apply the standard process of mutation and crossing in the genetic algorithm to obtain a subset of parameters with reasonable fitting.

Finally, we adjusted the parameters to obtain the best fit such that the amplitudes and periods in platelets are quantitatively consistent with the clinical data, and the qualitative properties of oscillation amplitude, period, and nadir level are satisfied for the neutrophil counts.

The resulting parameters for the two patients are given in Table 3.

Supplementary material

Supplementary material associated with this article can be found, in the online version, at 10.1016/j.jtbi.2018.11.024

References

Adimy, M., Angulo, O., Marquet, C., Sebaa, L., 2014. A mathematical model of multistage hematopoietic cell lineages. DCDS-B 19 (1), 1–26.

Apostu, R., Mackey, M.C., 2008. Understanding cyclical thrombocytopenia: a mathematical modeling approach.. J. Theor. Biol. 251 (2), 297–316.

Bernard, S., Bélair, J., Mackey, M.C., 2003. Oscillations in cyclical neutropenia: new evidence based on mathematical modeling.. J. Theor. Biol. 223 (3), 283–298.

Burns, F., Tannock, I., 1970. On the existence of a G_0-phase in the cell cycle.. Cell Prolif. 3 (4), 321–334.

Câmara De Souza, D., Craig, M., Cassidy, T., Li, J., Nekka, F., Bélair, J., Humphries, A.R., 2018. Transit and lifespan in neutrophil production: implications for drug intervention.. J Pharmacokinet. Pharmacodyn. 45 (1), 59–77.

Chang, Y., Bluteau, D., Debili, N., Vainchenker, W., 2007. From hematopoietic stem cells to platelets.. J. Thrombosis Haemostasis 5 (s1), 318–327.

Colijn, C., Mackey, M.C., 2005. A mathematical model of hematopoiesis—I. periodic chronic myelogenous leukemia.. J. Theor. Biol. 237 (2), 117–132.

Colijn, C., Mackey, M.C., 2005. A mathematical model of hematopoiesis: II. cyclical neutropenia.. J. Theor. Biol. 237 (2), 133–146.

Dale, D.C., Mackey, M.C., 2015. Understanding, treating and avoiding hematological disease: better medicine through mathematics? Bull. Math. Biol. 77 (5), 739–757.

Engelborghs, K., Luzyanina, T., Roose, D., 2002. Numerical bifurcation analysis of delay differential equations using DDE-BIFTOOL. ACM Trans. Math. Softw. 28 (1), 1–21.

Foley, C., Mackey, M.C., 2009. Dynamic hematological disease: a review.. J. Math. Biol. 58 (1), 285–322.

Fortin, P., Mackey, M., 1999. Periodic chronic myelogenous leukemia: spectral analysis of blood cell counts and aetiological implications. Br. J. Haematol. 104, 336–345.

Glass, L., Mackey, M., 1988. From clocks to chaos. Princeton University Press, Princeton, NJ.

Haurie, C., Dale, D.C., Mackey, M.C., 1998. Cyclical neutropenia and other periodic hematological disorders: a review of mechanisms and mathematical models. Blood 92 (8), 2629–2640.

Haurie, C., Dale, D.C., Mackey, M.C., 1999. Occurrence of periodic oscillations in the differential blood counts of congenital, idiopathic, and cyclical neutropenic patients before and during treatment with G-CSF. Exp. Hematol. 27 (3), 401–409.

Hoggatt, J., Kfoury, Y., Scadden, D.T., 2016. Hematopoietic stem cell niche in health and disease.. Annu. Rev. Pathol. 11, 555–581.

Horwitz, M., Benson, K.F., Person, R.E., Aprikyan, A.G., Dale, D.C., 1999. Mutations in ELA2, encoding neutrophil elastase, define a 21-day biological clock in cyclic haematopoiesis.. Nat. Genet. 23 (4), 433–436.

Kaushansky, K., Zhan, H., 2018. The regulation of normal and neoplastic hematopoiesis is dependent on microenvironmental cells.. Adv. Biol. Regul. 69, 11–15.

Kosugi, S., Tomiyama, Y., Shiraga, M., Kashiwagi, H., Nakao, H., Kanayama, Y., Kurata, Y., Matsuzawa, Y., 1994. Cyclic thrombocytopenia associated with igm anti-GPIIb-illa autoantibodies. Br. J. Haematol. 88 (4), 809–815.

Langlois, G.P., Arnold, D.M., Potts, J., Leber, B., Dale, D.C., Mackey, M.C., 2018. Cyclic thrombocytopenia with statistically significant neutrophil oscillations.. Clin. Case Rep. 6 (7), 1347–1352.

Langlois, G.P., Craig, M., Humphries, A.R., Mackey, M.C., Mahaffy, J.M., Bélair, J., Moulin, T., Sinclair, S.R., Wang, L., 2017. Normal and pathological dynamics of platelets in humans.. J. Math. Biol. 75 (6–7), 1411–1462.

Lei, J., Mackey, M.C., 2014. Understanding and treating cytopenia through mathematical modeling. In: A Systems Biology Approach to Blood. Springer, New York, pp. 279–302. Ch.14

Lei, J., Mackey, M.C., 2011. Multistability in an age-structured model of hematopoiesis: cyclical neutropenia. J. Theor. Biol. 270 (1), 143–153.

Lomb, N.R., 1976. Least-squares frequency analysis of unequally spaced data. Astrophys. Space Sci. 39 (2), 447–462.
Ma, S., Zhu, K., Lei, J., 2015. Bistability and state transition of a delay differential equation model of neutrophil dynamics. Int. J. Bifurcation Chaos 25 (1), 1550017.
Mackey, M.C., 1978. Unified hypothesis for the origin of aplastic anemia and periodic hematopoiesis.. Blood 51 (5), 941–956.
Mackey, M.C., 1979. Periodic auto-immune hemolytic anemia: an induced dynamical disease.. Bull. Math. Biol. 41 (6), 829–834.
MacLean, A.L., Filippi, S., Stumpf, M.P.H., 2014. The ecology in the hematopoietic stem cell niche determines the clinical outcome in chronic myeloid leukemia.. Proc. Natl. Acad. Sci. USA 111 (10), 3883–3888.
Morales-Mantilla, D.E., King, K.Y., 2018. The role of interferon-gamma in hematopoietic stem cell development, homeostasis, and disease.. Curr. Stem Cell Rep. 4 (3), 264–271.
Mouser, C.L., Antoniou, E.S., Tadros, J., Vassiliou, E.K., 2014. A model of hematopoietic stem cell proliferation under the influence of a chemotherapeutic agent in combination with a hematopoietic inducing agent.. Theor. Biol. Med. Model. 11, 4.
Nakamura-Ishizu, A., Takubo, K., Fujioka, M., Suda, T., 2014. Megakaryocytes are essential for hsc quiescence through the production of thrombopoietin.. Biochem. Biophys. Res. Commun. 454 (2), 353–357.
Pavord, S., Sivakumaran, M., Furber, P., Mitchell, V., 1996. Cyclical thrombocytopenia as a rare manifestation of myelodysplatic syndrome. Clin. Lab. Haematol. 18 (3), 221–223.
Pujo-Menjouet, L., 2016. Blood cell dynamics: half of a century of modelling. Math. Model. Nat. Phenom. 11 (1), 92–115.
Roeder, I., Herberg, M., Horn, M., 2009. An "age"structured model of hematopoietic stem cell organization with application to chronic myeloid leukemia. Bull. Math. Biol. 71 (3), 602–626.
Safarishahrbijari, A., Gaffari, A., 2013. Parameter identification of hematopoiesis mathematical model - periodic chronic myelogenous leukemia.. Contemp. Oncol. (Pozn) 17 (1), 73–77.
Santillán, M., Mahaffy, J.M., Bélair, J., Mackey, M.C., 2000. Regulation of platelet production: the normal response to perturbation and cyclical platelet disease. J. Theor. Biol. 206 (4), 585–603.
Sekine, T., Takagi, M., Uemura, Y., Mori, Y., Wada, H., Minami, N., Deguchi, K., Shirakawa, S., 1989. A cyclic thrombocytopenia associated with sjögren syndrome. Rinsho Ketsueki 30 (7), 1021–1026.
Seong, D., Thall, P., Kantarjian, H.M., Talpaz, M., Swantkowski, J., Xu, J., Shen, Y., Glassman, A., Ramagli, L., Siciliano, M.J., 1998. Philadelphia chromosome-positive myeloid cells in the peripheral blood of chronic myelogenous leukemia patients: comparison with the frequency detected in cycling cells of the bone marrow.. Clin. Cancer Res. 4 (4), 861–867.
Sieber, J., Engelborghs, K., Luzyanina, T., Samaey, G., Roose, D., 2014. DDE-BIFTOOL manual - bifurcation analysis of delay differential equations. http://arxiv.org/abs/1406.7144.
Swinburne, J.L., Mackey, M.C., 2000. Cyclical thrombocytopenia: characterization by spectral analysis and a review.. J. Theor. Med. 2 (2), 81–91.
Traulsen, A., Lenaerts, T., Pacheco, J.M., Dingli, D., 2013. On the dynamics of neutral mutations in a mathematical model for a homogeneous stem cell population.. J. R. Soc. Interface 10 (79), 20120810.
Wahlberg, P., Nyman, D., Ekelund, P.S.A.C., Granlund, H., 1977. Cyclical thrombocytopenia with remission during lynestrenol treatment in a woman. Ann. Clin. Res. 9 (6), 356–358.
Whichard, Z.L., Sarkar, C.A., Kimmel, M., Corey, S.J., 2010. Hematopoiesis and its disorders: a systems biology approach.. Blood 115 (12), 2339–2347.
Zhuge, C., Lei, J., Mackey, M.C., 2012. Neutrophil dynamics in response to chemotherapy and G-CSF. J. Theor. Biol. 293, 111–120.